Enhanced Energy Storage Performance of Lead-Free Capacitor in Ultra-widen Temperature range via Engineering Paraferroelectric and Relaxor Ferroelectric Multilayer Film

Tian-Yi Hu[a], Chunrui Ma[a,*], Yanzhu Dai[b], Qiaolan Fan[b], Ming Liu[b], Chun-Lin Jia[a,b,c]

[a] State Key Laboratory for Mechanical Behaviour of Materials and School of Materials Science and Engineering, Xi'an Jiaotong University, Xi'an, 710049, China

[b] School of Microelectronics, Xi'an Jiaotong University, Xi'an,710049, China

[c] Ernst Ruska Centre for Microscopy and Spectroscopy with Electrons, ForschungszentrumJülich, D-52425,Jülich, Germany

ABSTRACT

Industry has been seeking the thin film capacitor that can work at high temperature in harsh environment, where the cooling systems are not desired. Up to now, the working temperature of thin film capacitor is still limited up to 200 °C. Herein, we design a multilayer structure with layers of paraferroelectric ($Ba_{0.3}Sr_{0.7}TiO_3$, BST) and relaxor ferroelectric ($0.85BaTiO_3$-$0.15Bi(Mg_{0.5}Zr_{0.5})O_3$, BT-BMZ) to realize optimum properties with a flat platform of dielectric constant and high breakdown strength for excellent energy storage performance at high temperature. Through optimizing the multilayer structure, a highly stable relaxor ferroelectric state is obtained for the BST/BT-BMZ multilayer thin film capacitor with a total thickness of 230 nm, a period number N=8, and a layer thickness ratio of BST/BT-BMZ=3/7. The optimized multilayer film shows significantly improved energy storage density (up to 30.64 J/cm^3) and energy storage efficiency (over 70.93%) in ultra-wide temperature range from room temperature to 250 °C. Moreover, the multilayer system exhibits also excellent thermal stability in such ultra-wide temperature range with the change of 5.15%, and 12.75% for the recoverable energy density and energy storage efficiency, respectively. Our results demonstrate that the designed thin film capacitor is promising for the application in harsh environment and open a way to tailor thin film capacitor toward higher working temperature with enhanced energy storage performance.

KEYWORDS: Energy storage; High temperature; Lead-free thin film; Paraelectrics;

Relaxor ferroelectrics.

1. INTRODUCTION

Thin film capacitors as one type of the most important devices for energy storage applications have attracted much attention owing to the behavior of rapid charge/discharge and integration compatibility in the printed-circuit-board. These characteristics make them indispensable in advanced electronics, energy power generation system, inverter equipment of hybrid electric vehicle, and medical equipment.[1-3] With the development of electronic devices towards miniaturization, integration and lightweight, it is particularly important to improve the recoverable energy density (W_{re}) at high temperature and thermal stability of the capacitors.[4] One reason is the unavoidable fluctuation of the operating temperature within a certain range. The other reason is that the currently commercialized ceramic capacitors X7R, X8R, even X9R do not meet the temperature requirement (up to 250 °C) for the applications in control and sensing electronics placed near the outer shell of rockets and spaces shuttles, oil drilling and other harsh environmental conditions, where the cooling system may not be possible in these circumstances or the cooling is ineffective.[5] It is known that high breakdown strength and dielectric constant are two important parameters for energy storage. However, high temperature can aid the charge carrier transport or hop in the materials, making the capacitors easier to breakdown, and also randomize the dipole alignment and lead to decrease of dielectric constant. It seems impossible to obtain the high energy storage performance at high temperature. In order to solve the problem, several methods have been proposed to improve the energy storage performance of thin film capacitor at high temperature. One effective way is seeking a material with high thermal activation energy (hopping

energy barrier) to suppressed electron transport or a modified material by doping to reduce leakage current, and hence obtaining high breakdown strength at high temperature.[6,7] For example, Kwon *et al* found that the W_{re} of $0.88BaTiO_3$-$0.12Bi(Mg_{0.5}Ti_{0.5})O_3$ thin film is stable in the temperature range from 25 °C to 200 °C with a value of W_{re} ~8.0 J/cm^3.[8] Liang *et al* reported that $BaZr_{0.35}Ti_{0.65}O_3$ thin film not only exhibit high energy density at room temperature (up to 78.7 J/cm^3), which is higher than the $Pb_{0.92}La_{0.08}Zr_{0.52}Ti_{0.48}O_3$ film (67 J/cm^3 , at room temperature) reported by Ma *et al*,[9] but also exhibits good energy storage performance from -150 °C to 200 °C with the W_{re} up to 41.9 J/cm^3, which is even higher than the reported lead-based $Pb_{0.92}La_{0.08}Zr_{0.52}Ti_{0.48}O_3$ thin film in the high temperature range from room temperature to 180 °C .[10,11] Another effective way to boost the energy storage performance of thin film capacitors is to design composited or hetero-structural thin films by selecting suitable two or three material components. [12-14] Zhang *et al* designed a multilayer film composed of $0.7Na_{0.5}Bi_{0.5}TiO_3$-$0.3SrTiO_3$ with larger polarization and $0.6SrTiO_3$-$0.4Na_{0.5}Bi_{0.5}TiO_3$ with larger breakdown strength and achieve energy storage density up to 26 J/cm^3 and energy storage efficiency more than 60% from 20 °C to 180 °C.[15]

Although much effort have been made on optimizing lead-free materials, it is still the challenge work so far to increase the upper operation temperature boundary to 250 °C with reasonably high performances. In this paper, we propose a multilayer structure with paraelectric $Ba_{0.3}Sr_{0.7}TiO_3$ (BST) and relaxor ferroelectric $0.85BaTiO_3$-$0.15Bi(Mg_{0.5}Zr_{0.5})O_3$ (BT-BMZ) to achieve both high breakdown

strength and dielectric constant at high temperature. The component layer of BST is selected due to its lower Curie temperature (-103 °C), guaranteeing the paraelectric state or stable dielectric constant at high temperature.[16] Besides, its breakdown strength is the highest among the family of $Ba_{1-x}Sr_xTiO_3$.[17] For the other component layer, relaxor ferroelectric BT-BMZ ceramic exhibits a diffused phase transition from ferroelectric to paraelectric at around -25 °C under test frequency of 1 kHz with almost temperature-insensitive dielectric constant at high temperature.[18] Therefore, the combination of BST and BT-BMZ is expected to be a good candidate for high-temperature dielectric capacitor. Optimization of the multilayer structure leads to excellent thermal stability from room temperature (RT) to 250 °C with highly improved energy storage density W_{re} (up to 30.64 J/cm^3) and efficiency η (70.93%). Moreover, the changes of W_{re} and η in the test temperature range are within 5.15% and 12.75%, respectively, both of which satisfy the industry requirement ($\Delta W_{re}/W_{re}$, $\Delta\eta/\eta < \pm 15\%$).

2. EXPERIMENTAL SECTION

2.1 Fabrication of epitaxial thin films.

The epitaxial BST/BT-BMZ multilayers were grown on conductive (001) 0.7% Nb doped $SrTiO_3$ (Nb:STO) single-crystal substrates (a=3.905 Å), which acts as the bottom electrode, through a radio-frequency (RF) magnetron sputtering system. In order to optimize the energy storage performances, three types of multilayer films were designed with variation of (i) component ratio defined by thickness ratio (R) between the BST and BT-BMZ component layers, (ii) the repeat periods (N) of the

BST/BT-BMZ double layer, and (iii) the total thickness of the film system. A layer of BST is firstly deposited on the substrate considering its lattice constant close to that of the substrate.[19] The layer thickness ratio of the two compounds was controlled by growth time. All of the multilayer samples were fabricated at 700 °C under an Ar/O_2 mixture atmosphere with the mixed ratio of 1:1 and a total pressure of 0.20 mbar. The distance between the target and the substrate is fixed at 55 mm and the sputtering power is kept 100 W. After the deposition, the samples were *in-situ* annealed at 700 °C for 15 minus in an Ar/O_2 mixture atmosphere with the mixed ratio of 1:1 and a total pressure of 200 mbar, and then naturally cooled down to room temperature.

2.2 Characterization.

The phase and epitaxial nature of the multilayer samples were characterized using the high resolution X-ray diffraction (HRXRD) techniques including θ–2θ scan, φ scan, and reciprocal space mapping (RSM), on a PANalyticalX'Pert MRD with a radiation wavelength of 1.54 Å. The microstructure of the multilayer thin films was investigated by scanning transmission electron microscopy (STEM) on a JEOL ARM 200 F electron microscope. In order to measure the dielectric and ferroelectric properties of the samples, a Pt layer was deposited as the top electrode on the top of the samples by RF-sputtering with a 200 μm× 200 μm shadow mask. Agilent 4980A LCR impedance analyzer was used to characterize the dielectric constant and dielectric loss as a function of frequency (100 Hz~1 MHz) and temperature (25 °C~250 °C). The FORC loops and ferroelectric hysteresis loops (*P*-*E*) in the temperature range from 25 °C to 250 °C under frequency of 1 kHz were recorded by a

ferroelectric tester (TF2000 analyzer, axi ACCT, Aachen, Germany). The breakdown tests of the thin films were taken by applying a 1 kHz Triangular Wave electric field at room temperature. The different temperature environment was provided through Lakeshore cryo-cooled probe station (CRX-6.5K, Lake Shore Cryotronics, Inc., USA). The fast discharge experiments were carried out in a capacitor charge-discharge test system (PK-CPR 1701-15012, PolyK Technologies, PA, USA).

3. RESULTS AND DISCUSSION

Fig 1(a) is representative of XRD θ-2θ scans for BST single layer film, BT-BMZ single layer film and BST/BT-BMZ multilayer film (BST/BT-BMZ=3/7, 230 nm). Only the (00*l*) reflection peaks of these films and Nb:STO substrate can be found, demonstrating that all of the films are *c*-axis orientation. The φ scan measurements taken around the {101} reflections of the samples and the Nb:STO substrate were performed in order to investigate the epitaxial nature of the samples. As shown in Fig 1(b), the φ scan patterns of the BST, BT-BMZ and N=8 multilayer coincide with the pattern of Nb:STO substrate and all of them exhibit well-defined sharp peaks and four-fold symmetry. According to the patterns from θ-2θ and φ scan, the epitaxial relationship of the films is $(001)_{BT\text{-}BMZ} // (001)_{BST} // (001)_{Nb:STO}$ and $[100]_{BT\text{-}BMZ} // [100]_{BST} // [100]_{Nb:STO}$. From the STEM dark field images (Fig 1(c)), the interfaces between the heterolayers can be seen clearly and thus the feature of multilayers is confirmed. The insets of the Fig 1(c) show the corresponding selected area electron diffraction (SAED) patterns along the [100] zone axis of Nb:STO, and the arrangement of the diffraction spots from different layers further confirm the epitaxial

relationship. We also note from the images a common feature for all of the film systems that the first several film layers look flat and become wavy with increase of the thickness. The possible root is the strain effect induced by lattice misfit between BST and BT-BMZ, about ~1.87%. The strain is relaxed by dislocations with the increase of film thickness. The dislocations or defects in the film make the film orientation deviate in nanoscale, and generate the wavy surface, but all of the films macroscopically are (001) oriented.

The characteristic breakdown strength of the multilayer systems was first analyzed by the Weibull statistics. The influences of thickness ratio R between the BST and BT-BMZ layers, the repeat period number N and the total thickness on the breakdown strength were investigated by varying one of the effect factors and fixing another two factors. Fig 2(a) shows the breakdown strength of the multilayers for three representative component ratio values (R=1/9, 2/8 and 3/7) and fixed N=8 and the fixed total thickness ~230 nm. It can be see that the optimum ratio of BST/BT-BMZ is 3/7. The effect of repeat period number is investigated under fixed the ratio R=3/7 and total thickness ~230 nm. As shown in Fig 2(b), the breakdown strength first increases with the period number N and reaches the maximum value 7.90 MV/cm at N=8, and then slightly reduces to 6.99 MV/cm at N=12. As we previously reported, the interface of the multilayer can block propagation of the electric tree in the film. On the other hand, for a fixed total thickness of a multilayer system, the thickness of each component layer become thinner with the increased N, which makes the interface coupling stronger and the interface blocking effect

attenuated.[12,20] Fig 2(c) shows the impact of the total thickness on the breakdown strength. It was found that E_b first increases with total thickness, reaches the maximum value at ~230 nm, and then gradually decreases. This behavior is the result of competition between the effect of interface density and the effect of interfacial "dead layer". The "dead layer" plays a negative effect on the E_b, and this negative effect gradually decrease with increase of the sample thickness. On the other hand, with increase of thickness the density of the interfaces also decreases, attenuating the block effect on the propagation of electric tree. The E_b of the multilayer with the thickness of 460 nm is smaller than that of the sample with the thickness of 230 nm, demonstrating that the effect of the "dead layer" becomes attenuate and interface density plays a dominant role.[14] The competition between the "dead layer" and interface density generates the maximum value of E_b at 230 nm thickness. The W_{re} and η of these multilayers under the maximum electric field calculated based on unipolar *P-E* loop measured at RT (Fig S1-3) are summarized in Fig 2(d). It can be seen that at room temperature, the maximum W_{re} ~87.26 J/cm^3 with the η ~61.05% is achieved for the multilayer at BST/BT-BMZ =3/7, N=8 and total thickness of 230 nm. The bipolar *P-E* loops of the multilayer thin films were also measured as shown in the Fig S4(a-c) and the corresponding energy density and efficiency is summarized in Fig S4(d). The optimal energy storage properties are also achieved at the multilayer with BST/BT-BMZ =3/7, N=8 and total thickness of 230 nm and W_{re} is around 85.73 J/cm^3 and η is around 63.74%, which is almost the same as the energy storage performance under the unipolar electric field, so here we adopt unipolar *P-E* loop to investigate and

calculate the energy storage performance of the multilayers.

The maximum recoverable energy density of the optimized multilayer structure results from not only the maximum breakdown strength but also the contribution of medium dielectric constant. Fig 3(a-c) shows the dielectric constants for all of these samples as function of frequency at RT. It is expected that the dielectric constants decrease as the frequency increases considering that the dipoles are unable to keep pace with the change of the voltage at high frequency. This is proved from the increased dielectric loss at the corresponding frequency. The dielectric constant and the dielectric loss of the samples at 1 kHz and 1 MHz are extracted and shown in Fig 3(d). In the 1 kHz, it is found that the dielectric constant of the optimum multilayer exhibits the medium value rather than the highest value and the dielectric loss of the samples is less than 0.2 in the frequency range. Normally, it is expected that the difference in conductivity and dielectric constant between BST and BT-BMZ would generate concentrated charges at the interface, and thus induce dielectric constant increase as N increase.[21-23] However, in real materials the interfaces are usually not ideally sharp and local ion intermixture exists across the interfaces. In this case, as thickness of the component layer decreases, the effect of the ion intermixture at the interfaces becomes obvious and the interface polarization becomes indistinct, which finally induces the bound charge decrease and reduces the dielectric constant.[23] This behavior of ion intermixture can be tested by RSM of the multilayer samples (Fig S5). As shown in Fig S5, the peaks for the BST and BT-BMZ layers can be clearly seen at N=2 and the two peaks gradually merge together as the period number increases,

especially for N=12 sample. This indicates that when the period number is small, the BST and BT-BMZ layer exhibits the dielectric constant of itself phase, plus additional contribution from an interface polarization. As the period number increases, the effect of the ion mixture at the interfaces become severe, leading to the formation of composited phase/film of BST and BT-BMZ, and thus to the reduced dielectric constant. Therefore, the competition between the concentrated charge and the ion intermixture results in the medium dielectric constant for the optimal structure (BST/BT-BMZ=3/7, 230 nm, N=8). The dielectric properties at 1 MHz also are summarized in Fig 3(d) since it is more close to the intrinsic dielectric response. The dielectric constant variation trend of multilayer thin films at 1 MHz is the same as at 1 kHz, except the relative smaller dielectric constant, which is due to the contribution from the extrinsic factor, for example bound charge, decrease as the increased frequency. The same change trend of dielectric constant with interface number at 1 kHz and 1 MHz indicates that the dielectric constant is mainly determined by the interface number.

The behavior of dielectric constant also can be characterized by the first order reversal curve (FORC), which is an effective method to investigate the properties of polarization and the mechanism of domain switching, and directly determine the value of dielectric constant. The FORC distribution is derived from a series of FORC loops and the Preisach density $\rho(E_r, E)$ calculated by the $\rho(E_r, E) = \frac{1}{2}\frac{\partial P^2(E_r,E)}{\partial E_r \partial E}$, [24] where $P(E_r, E)$ is the polarization of the FORC loop, E is the real electric field and E_r is the reversal electric field. The Preisach density represents the density distribution of ideal

'hysteron' and provides the information of local switching behavior.[25,26] In this work, we set the E_{max}=3.9 MV/cm, ΔE_r=ΔE=0.13 MV/cm and 60 FORC loops were measured. The FORC distribution of the thin films N=4 and N=12 in Fig 4(b) exhibits a low-density distribution zone around the central region, which may be caused by domain wall motion or the domain wall switching in the low electric field and this can contribute to the large total polarization of thin films N=4 and N=12 in the Fig 4(a).[27,28] The shrinkage of the low-density distribution zone of N=8 implies less polarization nonlinear and more stable RFE (Relaxor Ferroelectric) state, since more stable RFE state always exhibit lower energy barrier for domain switching and lower coercive. Normally, the defects, strain or the interface of the thin film act as domain pinning centers and significantly influence the domain mobility and the energy barrier of the film.[26] As shown in Fig 1(c), the interfaces between the first several component layers are sharp and flat, and then gradually become undulating as the thickness of the film increases. The change in morphology of the interfaces may have effects on the properties. However, the common behave of the interface morphology is expect to result in similar effects on all of the film systems, and thus do not influence significantly the results of structure optimization. In the high-electric-field zones, the $\rho(E_r,E)$ intensity maintain a relatively evenly distributed, and values close to zero, since the high electric field can provide an energy to overcome the energy barrier and induce domain wall fully switching.[28]

As we mentioned above, the operating temperature is a key factor for the application of materials in the electronic devices. From the measurements of dielectric

constant and dielectric loss as function of temperature at 1 kHz (Fig 5(a)), we can see that the change of dielectric constant and dielectric loss of the optimum multilayer is only ~ 14.59% and 14.01%, respectively, from RT to 250 °C. These temperature-independent dielectric properties phenomenon can also found in other modified $Bi(Mg_{0.5}Ti_{0.5})O_3$ materials and it can be considered as the lower carriers transport or the re-entrant dipole glass-like relaxor behavior which caused by the ionic disorder and charge mismatch.[29-33] The dielectric loss of the multilayer film exhibits more stable and lower value (less than 0.1) than those of the single layer films of BST and BT-BMZ. These preeminent dielectric properties in such wide temperature are benefit for energy storage at high temperature. The W_{re} and η of these three samples as function of temperature are summarized in Fig 5(b), and the corresponding *P*-*E* loop is shown in Fig S6. It is exciting to see that the operating temperature of the optimum multilayer extends to 250 °C, compared to 150 °C of BST and 200 °C of BT-BMZ at the same electric field 3.0 MV/cm. Moreover, the W_{re} value is up to 30.64 J/cm^3, 30.01% and 12.73% higher than those of the single layer films of BST and BT-BMZ at their highest working temperature 150 °C and 200 °C, respectively(Fig S7). Especially, the W_{re} changes only ~ 5.15%, from 29.14 J/cm^3 at RT to 30.64 J/cm^3 at 250 °C, demonstrating a high thermal stability of the optimum multilayer system. The slight increase of the W_{re} value at the temperature range from 150-250 °C can be attributed to the small increase of the difference between the maximum polarization (P_m) and the remanent polarization (P_r) (Fig S6). Meanwhile, the change of energy storage efficiency η is ~ 12.75 % and remains above 70 % in the ultra-wide

temperature range, which is 58.35% and 13.62% higher than those of the single layer films of BST and BT-BMZ at their highest working temperature 150 °C and 200 °C, respectively. The high η can be related to the relatively low leakage current at high temperature illustrated in Fig 5(c). These properties of the optimal multilayer system satisfy the requirement for the stability and efficiency ($\Delta W_{re}/W_{re}$, $\Delta\eta/\eta < \pm 15\%$, and $\eta \geq 70$ %) in applications by industry and the working temperature range is much wider than those reported for the other lead-free systems, as shown in Fig 5(d).[8,10,20,34-36] Besides the high recoverable energy density and energy storage efficiency, a great power density of 0.27 MW/cm^3 has also been obtained for the optimal multilayer system at 250 ^{o}C under the electric field of 1.74 MV/cm, as shown in Fig 5(e). These excellent energy storage performances from 25 ^{o}C to 250 ^{o}C demonstrate that the capacitors not only have capability to store large electric energy than other type devices for energy storage applications, but also can deliver the energy in microseconds as shown in Fig 5(f).[2,12]

4 CONCLUSIONS

In summary, both the operation temperature and the energy storage performance (including energy storage density and efficiency) are largely improved by delicately designing the multilayer systems based on paraelectric BST and relaxor ferroelectric BT-BMZ. Investigations of this system demonstrate that the energy storage properties are related to the effective factors including the interface density, the thickness ratio between BST and BT-BMZ component layers, and total thickness of the film systems. Optimization between these factors leads to an optimal performance at N=8,

BST/BT-BMZ=3/7, and 230 nm total thickness. The optimal structure is of benefit to domain switch and hence exhibits less nonlinear polarization and more stale RFE state, which leads to extension of working temperature up to 250 °C with improved W_{re} (to 30.64 J/cm^3) and energy storage efficiency (up to 70.93%). Moreover, a superior thermal stability for the system is achieved in the ultra-wide temperature range from RT to 250 °C. These enhanced energy storage performances demonstrate that our proposed method is an effective and feasible way to improve the three key parameters (working temperature, energy storage density and energy storage efficiency) for devices for energy storage applications, and make them promising material systems for applications in harsh environment without the cooling system.

ASSOCIATED CONTENT

Supporting Information. Details of Weibull statistical failure analysis; Unipolar *P-E* loops, bipolar *P-E* loops of the multilayer films and the corresponding recoverable energy density and energy storage efficiency calculated based on *P-E* loop; RSM(Reciprocal space maps) of the multilayer films(N=2,4,8,12); the P_m-P_r under different temperature of the BST single layer thin film, BT-BMZ single layer thin film and the optimal BST/BT-BMZ multilayer thin film.

AUTHOR INFORMATION

Corresponding authors:

*E-mail addresses: chunrui.ma@xjtu.edu.cn(C.R. Ma).

NOTES

The authors declare no competing financial interest.

ACKNOWLEDGMENTS

This research is supported by Natural Science Foundation of China (No. 51702255 and 51390472), National “973” projects of China (No. 2015CB654903, No. 2015CB654603), Shaanxi Natural Science Foundation 2018JM5069, and Fundamental Research Funds for the Central Universities.

REFERENCES

(1) Yao, Z.; Song, Z.; Hao, H.; Yu, Z.; Cao, M.; Zhang, S.; Lanagan, M. T.; Liu, H. Homogeneous/Inhomogeneous-Structured Dielectrics and their Energy-Storage Performances. *Adv. Mater.* **2017**, *29* (20), 1601727.

(2) Palneedi, H.; Peddigari, M.; Hwang, G. T.; Jeong, D. Y.; Ryu, J. High-Performance Dielectric Ceramic Films for Energy Storage Capacitors: Progress and Outlook. *Adv. Funct. Mater.* **2018**, *28* (42), 1803665.

(3) Silva, José P. B.; Silva, João M. B.; Oliveira, Marcelo J. S.; Weingärtner, Tobias.; Sekhar, Koppole C.; Pereira, Mário.; Gomes, Maria J. M. High-Performance Ferroelectric–Dielectric Multilayered Thin Films for Energy Storage Capacitors. *Adv. Funct. Mater.* **2018**, *29* (6), 1807196.

(4) Li, Q.; Chen, L.; Gadinski, M. R.; Zhang, S.; Zhang, G.; Li, H. U.; Iagodkine, E.; Haque, A.; Chen, L. Q.; Jackson, T. N.; Wang, Q. Flexible high-temperature dielectric materials from polymer nanocomposites. *Nature* **2015**, *523*, 576–579.

(5) Li, Q.; Yao, F. Z.; Liu, Y.; Zhang, G.; Wang, H.; Wang, Q. High-Temperature Dielectric Materials for Electrical Energy Storage, *Annu. Rev. Mater. Res*. **2018**, *48*, 219-243.

(6) Liang, Z.; Ma, C.; Shen, L.; Lu, L.; Lu, X.; Lou, X.; Liu, M.; Jia, C. L. Flexible lead-free oxide film capacitors with ultrahigh energy storage performances in extremely wide operating temperature. *Nano Energy*. **2019**, *57*, 519-527.

(7) Jiang, X.; Hao, H.; Zhang, S.; Lv, J.; Cao, M.; Yao, Z.; Liu, H. Enhanced energy storage and fast discharge properties of $BaTiO_3$ based ceramics modified by $Bi(Mg_{1/2}Zr_{1/2})O_3$. *J. Eur. Ceram. Soc.* **2019**, *39* (4), 1103-1109.

(8) Kwon, D. K.; Lee, M. H. Temperature Stable High Energy Density Capacitors using Complex Perovskite Thin Films. *IEEE Trans. Ultrason. Ferroelectr. Freq.*

Control. **2012**, *59*, 1894–1899.

(9) Ma, B.; Narayanan, M.; Liu, S.; Hu, Z.; Balachandran, U. Development of PLZT film-on-foil capacitors with high energy density. *J. Phys. Conf. Ser.* **2013**, *472*, 012004

(10) Liang, Z.; Liu, M.; Ma, C.; Shen, L.; Lu, L.; Jia, C. L. High-performance $BaZr_{0.35}Ti_{0.65}O_3$ thin film capacitors with ultrahigh energy storage density and excellent thermal stability. *J. Mater. Chem. A* **2018**, *6* (26), 12291-12297.

(11) Hu, G.; Ma, C.; Wei, W.; Sun, Z.; Lu, L.; Mi, S. B.; Liu, M.; Ma, B.; Wu, J.; Jia, C. L. Enhanced energy density with a wide thermal stability in epitaxial $Pb_{0.92}La_{0.08}Zr_{0.52}Ti_{0.48}O_3$ thin films. *Appl. Phys. Lett.* **2016**, *109* (19), 193904.

(12) Fan, Q.; Liu, M.; Ma, C.; Wang, L.; Ren, S.; Lu, L.; Lou, X.; Jia, C. L. Significantly enhanced energy storage density with superior thermal stability by optimizing $Ba(Zr_{0.15}Ti_{0.85})O_3/Ba(Zr_{0.35}Ti_{0.65})O_3$ multilayer structure. *Nano Energy* **2018**, *51*, 539-545.

(13) Fan, Q.; Ma, C.; Li, Y.; Liang, Z.; Cheng, S.; Guo, M.; Dai, Y.; Ma, C.; Lu, L.; Wang, W.; Wang, L.; Lou, X.; Liu, M.; Wang, H.; Jia, C. L. Realization of high energy density in an ultra-wide temperature range through engineering of ferroelectric sandwich structures. *Nano Energy* **2019**, *62*, 725-733.

(14) Sun, Z.; Wang, L.; Liu, M.; Ma, C.; Liang, Z.; Fan, Q.; Lu, L.; Lou, X.; Wang, H.; Jia, C. L. Interface thickness optimization of lead-free oxide multilayer capacitors for high-performance energy storage. *J. Mater. Chem. A* **2018**, *6* (4), 1858-1864.

(15) Zhang, Y.; Li, W.; Xu, S.; Wang, Z.; Zhao, Y.; Li, J.; Fei, W. Interlayer coupling to enhance the energy storage performance of $Na_{0.5}Bi_{0.5}TiO_3$–$SrTiO_3$ multilayer films with the electric field amplifying effect. *J. Mater. Chem. A* **2018**, *6* (47), 24550-24559.

(16) Shirokov, V. B.; Yuzyuk, Yu. I.; Dkhil, B.; Lemanov, V. V. Phenomenological

theory of phase transitions in epitaxial $Ba_xSr_{1-x}TiO_3$ thin films. *Phys. Rev. B.* **2009**, *79*, 144118.

(17) Wu, T.; Pu, Y.; Gao, P.; Liu, D. Influence of Sr/Ba ratio on the energy storage properties and dielectric relaxation behaviors of strontium barium titanate ceramics. *J. Mater. Sci-Mater. El.* **2013**, *24* (10), 4105-4112.

(18) Yuan, Q.; Li, G.; Yao, F. Z.; Cheng, S. D.; Wang, Y.; Ma, R.; Mi, S. B.; Gu, M.; Wang, K.; Li, J. F.; Wang, H. Simultaneously achieved temperature-insensitive high energy density and efficiency in domain engineered $BaTiO_3$-$Bi(Mg_{0.5}Zr_{0.5})O_3$ lead-free relaxor ferroelectrics. *Nano Energy* **2018**, *52*, 203-210.

(19) Yustanti, E.; Hafizah, M. A. E.; Manaf, A. Synthesis of strontium substituted barium titanate nanoparticles by mechanical alloying and high power ultrasonication destruction. *AIP Conf. Proc*. **2016**, *1725*, 020102.

(20) Sun, Z.; Ma, C.; Liu, M.; Cui, J.; Lu, L.; Lu, J.; Lou, X.; Jin, L.; Wang, H.; Jia, C. L. Ultrahigh Energy Storage Performance of Lead-Free Oxide Multilayer Film Capacitors via Interface Engineering. *Adv. Mater.* **2017**, *29* (5), 1604427.

(21) Fu, J.; Hou, Y.; Zheng, M.; Zhu, M. Dielectric and energy harvesting properties of $FeTiNbO_6$/PVDF composites with reinforced sandwich structure. *Polym. Composite.* **2019**, *40* (S1), E570-E578.

(22) Okatan, M. B.; Mantese, J. V.; Alpay, S. P. Polarization coupling in ferroelectric multilayers. *Phys. Rev. B* **2009**, *79* (17), 174113.

(23) Hou, C.; Huang, W.; Zhao, W.; Zhang, D.; Yin, Y.; Li, X. Ultrahigh Energy Density in $SrTiO_3$ Film Capacitors. *ACS Appl. Mater. Interfaces* **2017**, *9*, 20484-20490.

(24) Piazza, D.; Stoleriu, L.; Mitoseriu, L.; Stancu, A.; Galassi, C. Characterisation of porous PZT ceramics by first-order reversal curves (FORC) diagrams. *J. Eur. Ceram.*

Soc. **2006**, *26*, 2959-2962.

(25) Goh, Y.; Jeon, S. First-order reversal curve diagrams for characterizing ferroelectricity of $Hf_{0.5}Zr_{0.5}O_2$ films grown at different rates. *J. Vac. Sci. Technol. B*. **2018**, *36*, 052204.

(26) Wang, C.; Yang, X.; Wang, Z.; He, C; Long, X. Investigation of switching behavior of acceptor-doped ferroelectric ceramics. *Acta Mater.* **2019**, *170*, 100-108.

(27) Pan, H.; Ma, J.; Ma, J.; Zhang, Q.; Liu, X.; Guan, B.; Gu, L.; Zhang, X.; Zhang, Y. J.; Li, L.; Shen, Y.; Lin, Y. H.; Nan, C. W. Giant energy density and high efficiency achieved in bismuth ferrite-based film capacitors via domain engineering. *Nat. Commun.* **2018**, *9* (1), 1813.

(28) Lin, Y.; Li, D.; Zhang, M.; Zhan, S.; Yang, Y.; Yang, H.; Yuan, Q. Excellent Energy Storage Properties Achieved in $BaTiO_3$-based Lead-Free Relaxor Ferroelectric Ceramics via Domain Engineering on the Nanoscale. *ACS Appl. Mater. Interfaces* **2019**, *29*, 36824-36830.

(29) Chen, Z.; Li, G.; Sun, X.; Liu, L.; Fang, L. La_2O_3 modified $0.4(Ba_{0.8}Ca_{0.2})TiO_3$-$0.6Bi(Mg_{0.5}Ti_{0.5})O_3$ ceramics for high-temperature capacitor applications. *Ceram. Int.* **2015**, *41*(9), 11057-11061.

(30) Liu, X.; Liu, L.; Han, F.; Liu, S.; Xiang, H.; Fang, L. Dielectric behavior of La_2O_3-modified $0.4(Ba_{0.8}Ca_{0.2})TiO_3$-$0.6Bi(Mg_{0.5}Ti_{0.5})O_3$ lead-free ceramics. *J. Mater. Sci-Mater. El.* **2016**, *27* (11), 12128-12133.

(31) Ren, S.; Chen, Z.; Yan, T.; Han, F.; Kuang, X.; Fang, L.; Liu, L. High temperature dielectrics and defect characteristic of (Nb, Mn, Zr) modified $0.4(Ba_{0.8}Ca_{0.2})TiO_3$-$0.6Bi(Mg_{0.5}Ti_{0.5})O_3$ ceramics. *J. Phys. Chem. Solids* **2018**, *118*, 99-108.

(32) Xu, M.; Peng, B.; Zhu, J.; Liu, L.; Sun, W.; Leighton, G. J. T.; Shaw, C.; Luo, N.;

Zhang, Q. Enhanced energy storage performance of (1-x)(BCT-BMT)-xBFO lead-free relaxor ferroelectric ceramics in a broad temperature range. *J. Alloy. Compd.* **2019**, *789*, 303-312.

(33) Chen, K.; Fu, W.; Liu, J.; Yan, T.; Lan, Z.; Fang, L.; Peng, B.; Wang, D.; Liu, L. Re-entrant dipole glass-like behavior and lattice dynamics of $0.65Bi(Mg_{1/2}Ti_{1/2})O_3$-$0.35PbTiO_3$. *J. Am. Ceram. Soc.* **2019**, *103* (4), 2859-2867.

(34) Park, M. H.; Kim, H. J.; Kim, Y. J.; Moon, T.; Kim, K. D.; Hwang, C. S. Thin $Hf_xZr_{1-x}O_2$ Films: A New Lead-Free System for Electrostatic Supercapacitors with Large Energy Storage Density and Robust Thermal Stability. *Adv. Energy Mater.* **2014**, *4* (16), 1400610.

(35) Pan, H.; Zeng, Y.; Shen, Y.; Lin, Y. H.; Ma, J.; Li, L.; Nan, C. W. $BiFeO_3$–$SrTiO_3$ thin film as a new lead-free relaxor-ferroelectric capacitor with ultrahigh energy storage performance. *J. Mater. Chem. A* **2017**, *5* (12), 5920-5926.

(36) Pan, H.; Li, F.; Liu, Y.; Zhang, Q.; Wang, M.; Lan, S.; Zheng, Y.; Ma, J.; Gu, L.; Shen, Y.; Yu, P.; Zhang, S.; Chen, L. Q.; Lin, Y. H.; Nan, C. W. Ultrahigh-energy density lead-free dielectric films via polymorphic nanodomain design. *Science* **2019**, *365* (6453), 578-582.

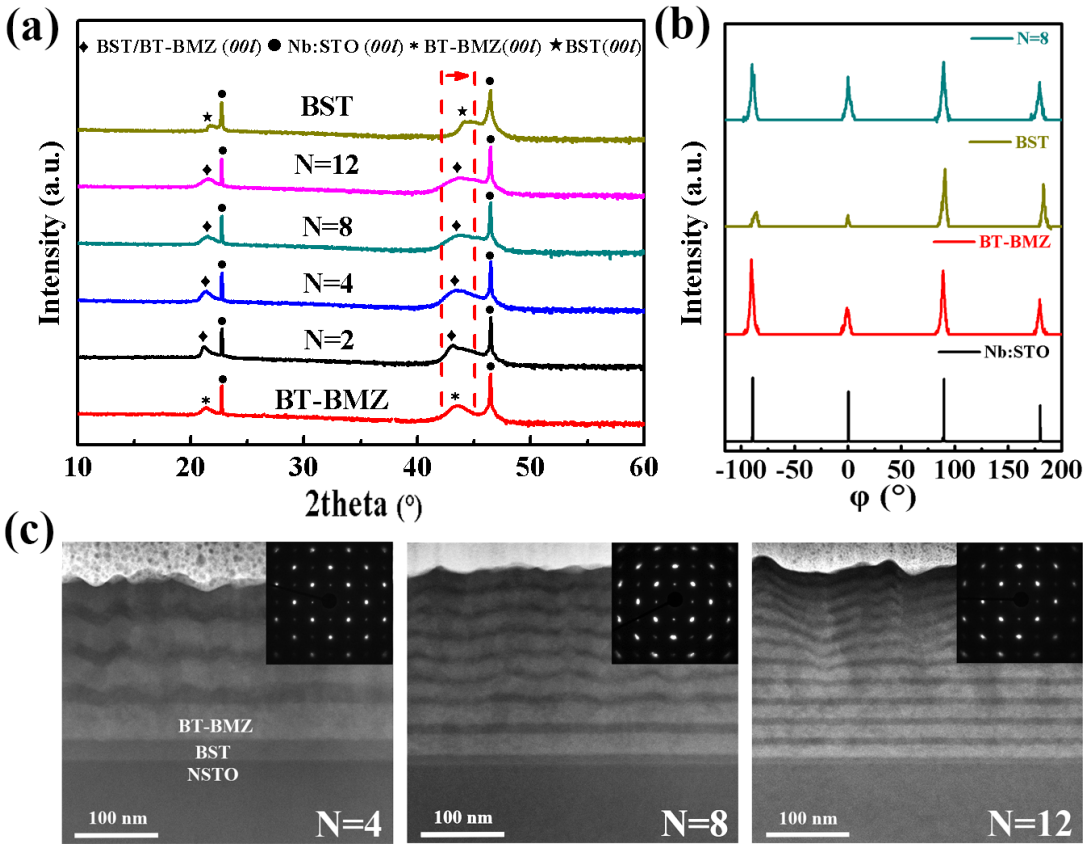

Fig 1. (a) Typical XRD *θ-2θ* scanning patterns for the BST single layer film, BT-BMZ single layer film and BST/BT-BMZ multilayer film (BST/BT-BMZ=3/7, total thickness 230 nm, N=2, 4, 8, 12) grown on (001) Nb:STO substrates. (b) φ-scans taken around the {101} reflection of the N=8 BST/BT-BMZ multilayer film, BT-BMZ single layer film, BST single layer film and Nb:STO substrate. (c) Cross-sectional STEM dark field images and corresponding selected area electron diffraction (SAED) patterns of the BST/BT-BMZ multilayers with N=4, 8, and 12.

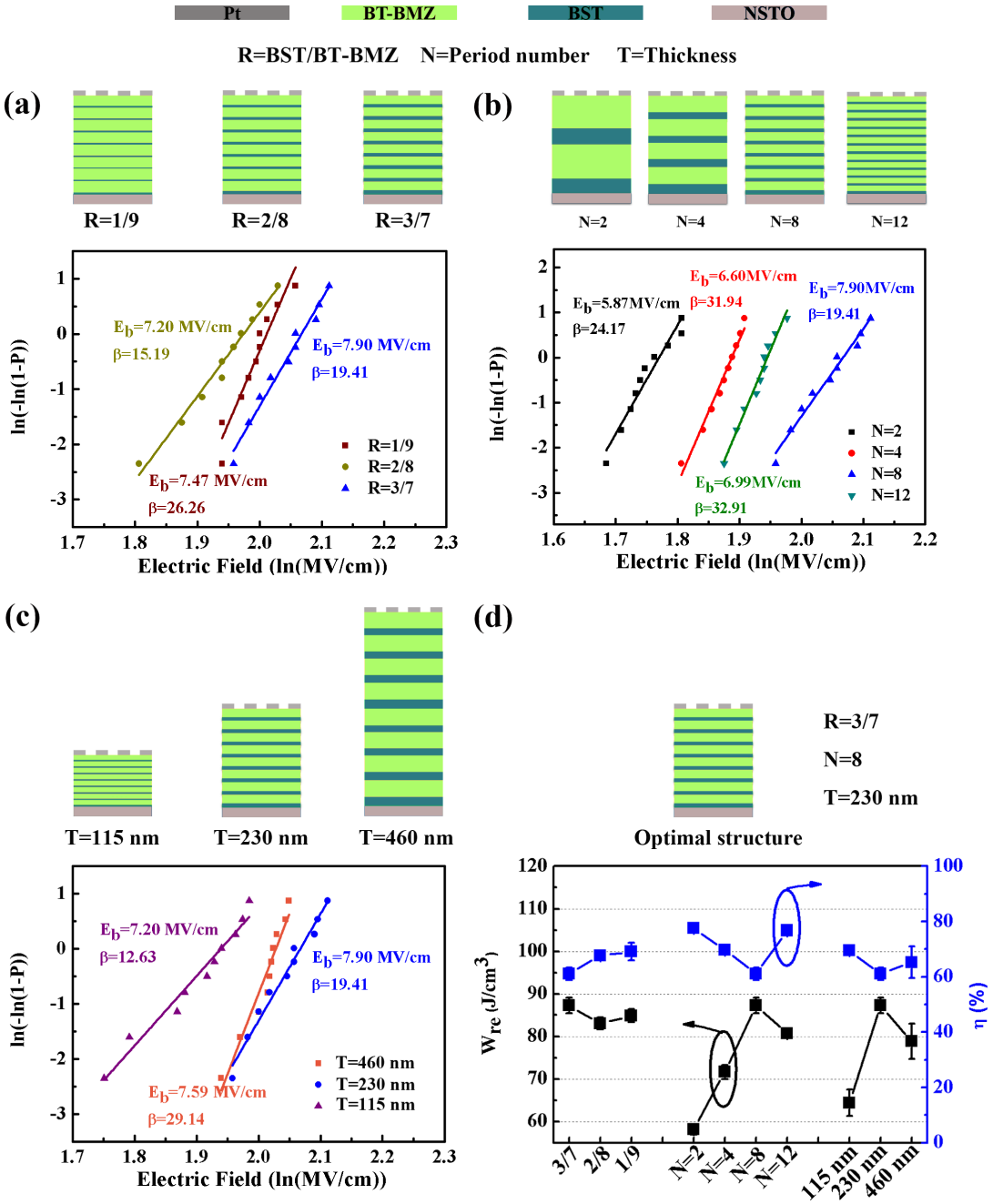

Fig 2. Sketch of the multilayer structures and corresponding Wei-bull distribution for the dielectric breakdown strength (a) for the films with component ratio R=1/9, 2/8, and 3/7, the fixed total thickness (230 nm) and period number (N=8), (b) for the films with period number N=2, 4, 8 and 12, the fixed total thickness (230 nm) and component ratio (R=3/7), (c) for the films with the total thicknesses of 115, 230 and 460 nm, the fixed component ratio (R=3/7) and period number (N=8). (d) Energy recoverable density (W_{re}) and energy storage efficiency (η) of all the BST/BT-BMZ multilayer films.

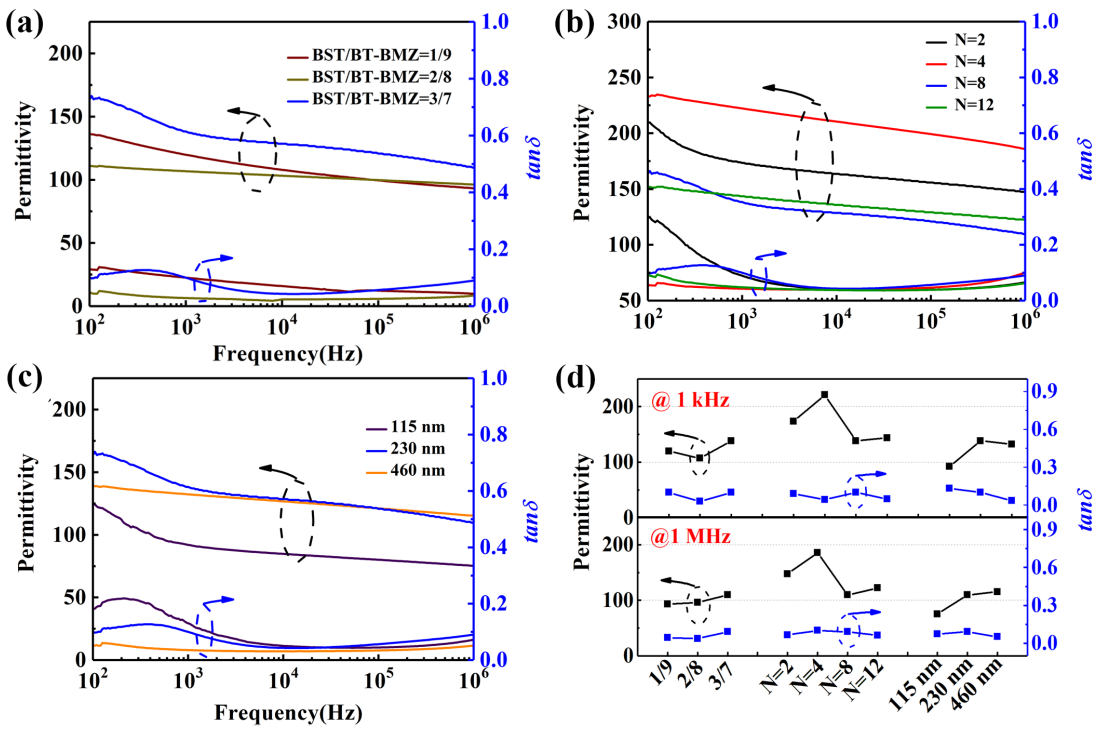

Fig 3. (a-c) Dielectric constant and dielectric loss depend on frequency for the multilayer films shown in Fig 2 at room temperature. (d) Dielectric constant and dielectric loss for all of the multilayer films at 1 kHz and 1 MHz.

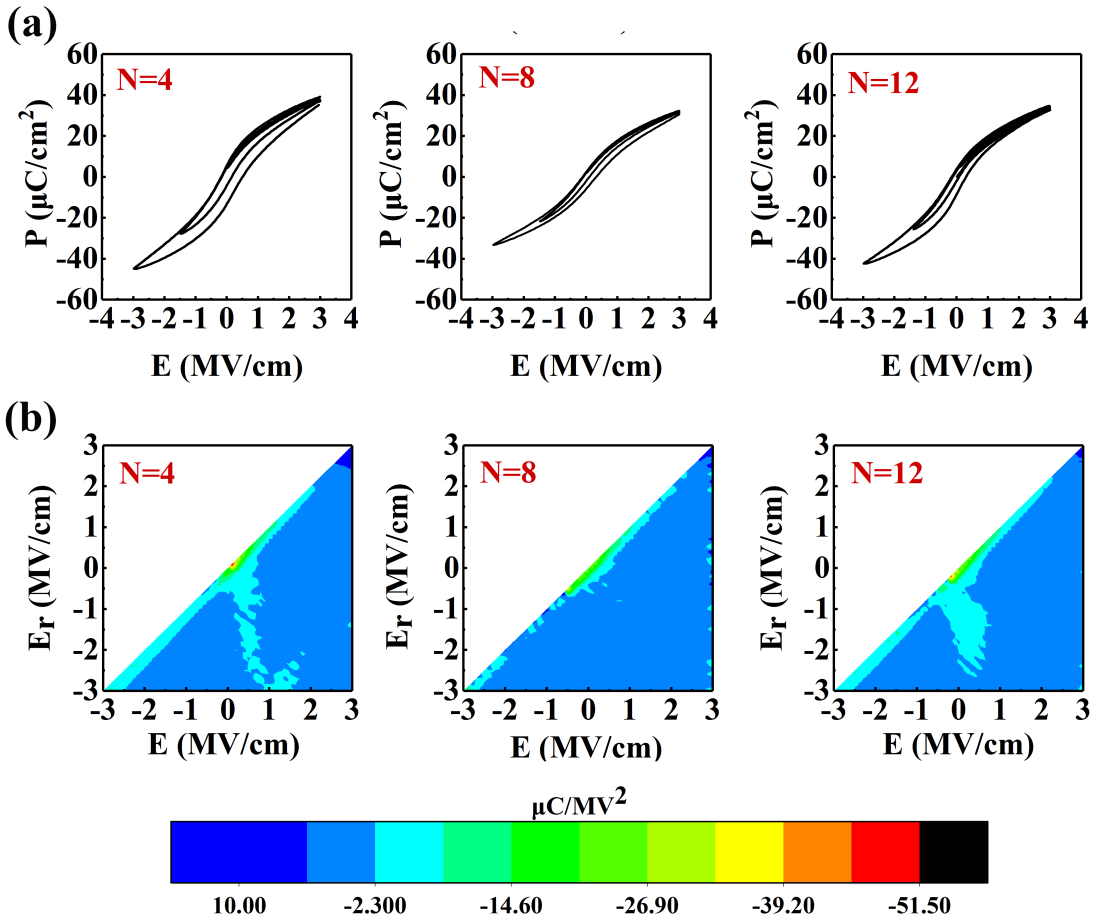

Fig 4. (a) FORC loops of the multilayer thin films with 230 nm, BST/BT-BMZ=3/7, N=4, 8 and 12. (Only 4 out of the total 60 loops are shown for clarity) (b) The corresponding FORC distribution $\rho(E_r,E)$ of the multilayer thin films.

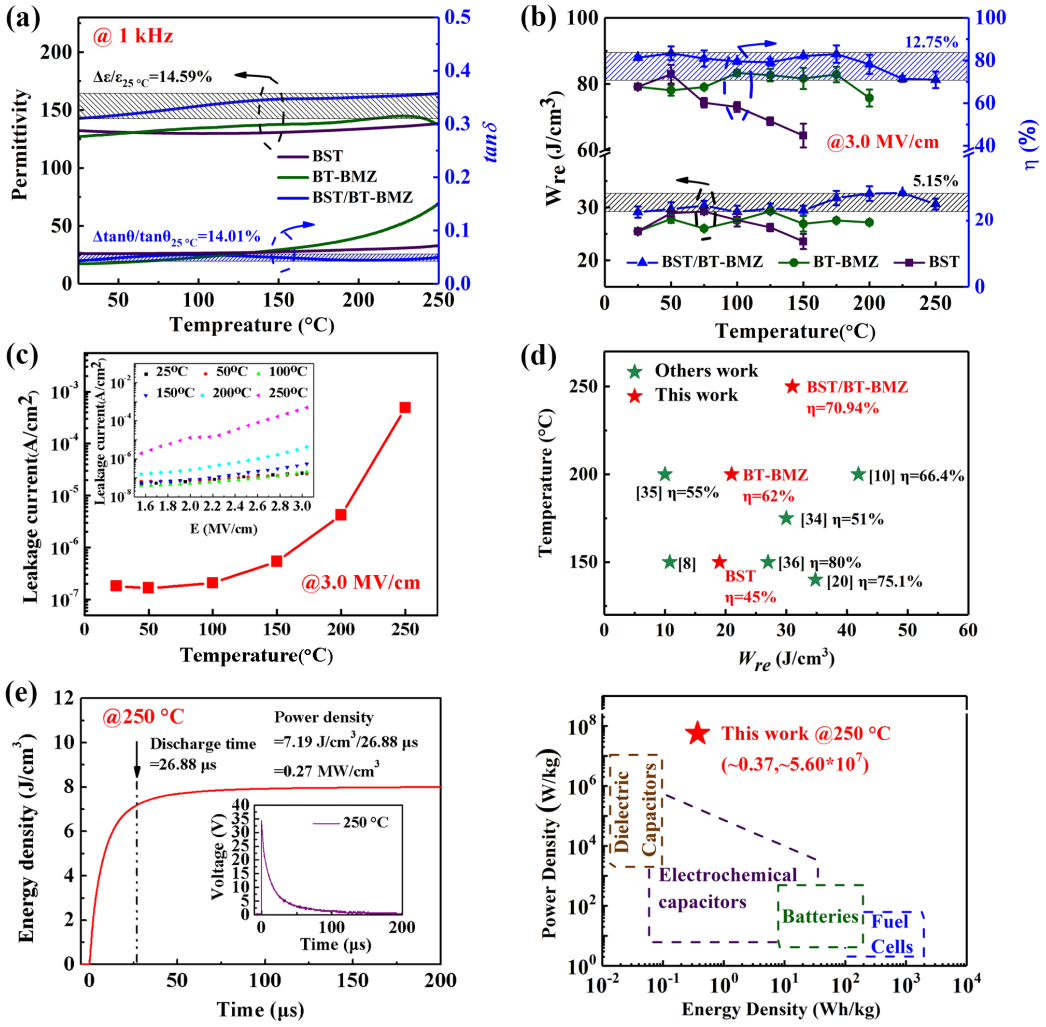

Fig 5. (a) Dielectric constant and dielectric loss of BST single layer film (230 nm), BT-BMZ single layer film (230 nm) and the optimal BST/BT-BMZ multilayer film (R=3/7, N=8, total thickness 230 nm) at 1 kHz as a function of temperature. (b) W_{re} and η depending on temperature for BST single layer film, BT-BMZ single layer film and the optimal BST/BT-BMZ multilayer at fixed electric field 3.0 MV/cm. (c) The leakage current of the optimal BST/BT-BMZ multilayer as a function of temperature under 3.0 MV/cm. The inset is leakage current *vs* electric field at different temperature. (d) The maximum working temperature of recently reported lead-free thin film capacitor with W_{re} and η respectively. (e) Discharge energy density as a function of time for the optimal multilayer film at 250 °C (under electric field of 1.74 MV/cm and the resistor load RL=100 kΩ). The inset shows the discharge voltage as function of time. (f) Comparison of the energy density and power density of typical electrical energy-storage devices.

TOC Graphic

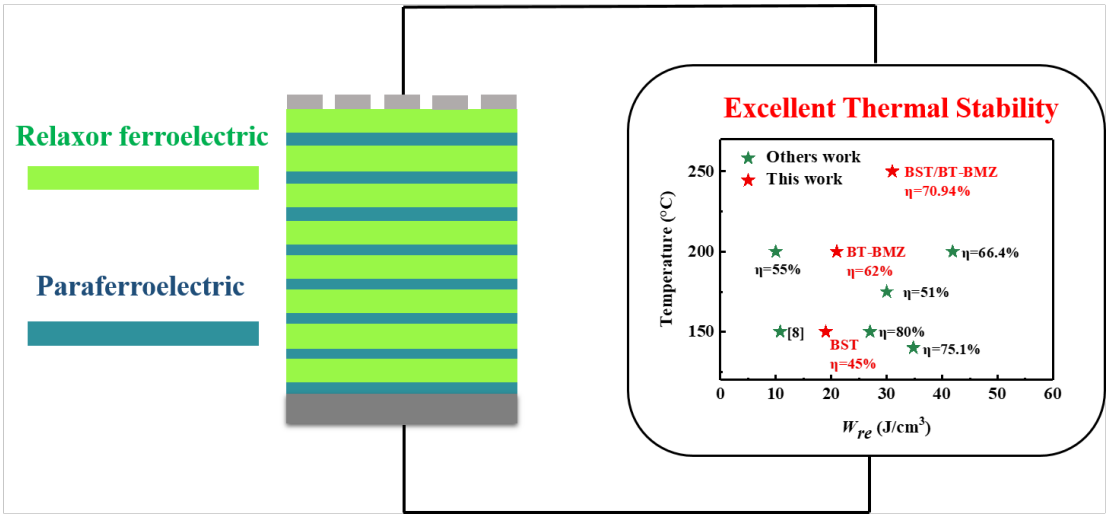

Supporting Information

Enhanced Energy Storage Performance of Lead-Free Capacitor in Ultra-widen Temperature range via Engineering Paraferroelectric and Relaxor Ferroelectric Multilayer Film

Tian-Yi Hu[a], Chunrui Ma[a,*], Yanzhu Dai[b], Qiaolan Fan[b], Ming Liu[b], Chun-Lin Jia[a,b,c]

[a] State Key Laboratory for Mechanical Behaviour of Materials and School of Materials Science and Engineering, Xi'an Jiaotong University, Xi'an, 710049, China

[b] School of Microelectronics, Xi'an Jiaotong University, Xi'an,710049, China

[c] Ernst Ruska Centre for Microscopy and Spectroscopy with Electrons, ForschungszentrumJülich, D-52425,Jülich, Germany

Corresponding authors:

*E-mail addresses: chunrui.ma@xjtu.edu.cn(C.R. Ma).